Fast And Accurate 3D Rendering Of Automotive Coatings

Eric Kirchner, Ivo van der Lans (1), Alejandro Ferrero (2), Joaquín Campos (2), Francisco M. Martínez-Verdú (3), Esther Perales (3). (1) Color Research, BA Performance Coatings, AkzoNobel, Sassenheim, the Netherlands, (2) Instituto de Óptica, Consejo Superior de Investigaciones Científicas (CSIC), c/Serrano 144, Madrid 28006, Spain, (3) Department of Optics, Pharmacology and Anatomy, University of Alicante, Carretera de San Vicente del Raspeig s/n 03690, Alicante, Spain.

Abstract

The color of automotive coatings varies with illumination and detection angles. For 3D rendering of these coatings currently two categories of methods exist, aiming at either color accuracy or at computational speed. Current methods that aim for color accuracy are based on measurement data from BRDF instruments. Since many hundreds of measurement geometries are needed to capture the color variation with angles, these methods require time-expensive interpolation of large three-dimensional Look-Up Tables. Current methods that aim for computational speed use physically crude approximations, usually taking into account color variations with respect to only one of the four angular dimensions.

Here, we derive a new approach for 3D rendering of automotive and other gonio-apparent coatings, which is a dedicated form of microfacet models. It aims at improved color accuracy as compared to the current computationally inexpensive methods, combined with higher computational speed and lower cost as compared to current color-accurate rendering techniques. The new approach utilizes a recently developed physical analysis method, introducing flake-based parameters and isochromatic lines, for the reflection properties of automotive coatings. This makes it more accurate than current fast rendering methods. The new method naturally leads to two- rather than three-dimensional Look Up Tables, which explains the small computation time it needs. We show that when applied to 3D rendering, this method indeed leads to accurate 3D rendering of automotive coatings while requiring reduced computation times. For numerical errors found in some special cases, solutions are found and tested.

Introduction

The technology for 3D rendering has developed fast over the past decades. Computer generated images of 3D scenes have become commonplace in the movie industry, advertisements and many other business areas. Because of a strong increase in computing power and software sophistication, the resulting images often suggest a photorealistic quality. Notwithstanding how striking the images thus produced often are, they are often not realistic [1], and the color accuracy is not good enough for critical applications such as automobile design [2].

Effect coatings such as metallic and interference paints are increasingly used in the automotive industry, packaging, consumer electronics, cosmetics etc. To render a three-dimensional object such as a car that carries this type of paint, the algorithms need to account for the fact that the color of these materials varies strongly with viewing and illumination angles. Generally, reflectance depends on the polar angle θ_{ill} of illumination, and on the polar angle θ_{det} and the azimuthal angle ϕ_{det} of the detector (or camera/observer). Therefore often the reflectance properties of the material are measured for a large number of combinations of these three angles. For this goal, special BRDF instruments are commercially available. For accurate sampling of each of the three angles, at least a few hundred measurement geometries are needed.

For 3D rendering purposes, the reflection properties need to be determined at each surface element, with local values for the illumination and detection angles θ_{ill}, θ_{det} and ϕ_{det}. For accurate 3D rendering purposes, this requires interpolation of the large three-dimensional Look Up Table representing the set of BRDF measurement data. This explains why for 3D rendering of automotive coatings, current methods that aim for high color accuracy are expensive in terms of computational time and required data storage. Obviously, several alternative models have been proposed in the past to reduce computation times and memory requirements, such as the well-known reflection models from Phong, Blinn, Ward and Cook-Torrance [3]. Although these models represent various levels of accuracy, they all involve the rather crude physical approximation that the angular variation of the reflectance is assumed to depend on only one angular parameter (only anisotropic microfacet models such as the one from Ashikhmin and Shirley [3] use two angular parameters like the one proposed here).

This approximation is also made when assuming that the angular variation of reflectance can be described as a function of aspecular angle (i.e. the angle with respect to the mirror angle) only. This approach was taken for 3D rendering applications by e.g. Meyer, Dumont-Bècle and others [4][5][6]. That approach has the advantage that the full 3D rendering can be based on reflection measurements at only a few measurement geometries from common multi-angle spectrophotometers. By interpolating the reflection data using the aspecular angle as the only parameter, a 3D rendering approach is thus formulated that is computationally fast, does not require much storage space, and uses a common multi-angle spectrophotometer rather than expensive BRDF instrumentation. We note that the Blinn model and the Torrance-Sparrow model have the same advantage.

However, the assumption that reflection properties depend only on the aspecular angle is far from exact. Even for metallic coatings this assumption easily leads to quantitative errors as large as $dE_{ab} = 5$ to 10 (for examples see e.g. Figure 5 in Ref.[7]). For a qualitative visualization of the lightness flop effect of metallic coatings this level of accuracy may be adequate. But especially for the interference pigments that are part of many automotive coatings, the assumption that reflection properties depend only on the aspecular angle is very crude. For example, Cramer showed how the reflective properties of coatings containing interference pigments vary strongly ($dE_{ab} > 30$) with illumination angle, even when the aspecular angle is kept constant [8]. For such coatings, all three color dimensions have such a subtle dependence on illumination and detection angles that it cannot be effectively parametrized by aspecular angle only.

In the present paper we propose an alternative approach that provides color-accurate results in a way that does not require much

computation time. The new approach is based on so-called isochromatic lines, a concept that is reviewed in section 2. Its application to 3D rendering is discussed in section 4. In section 3 we introduce color maps as a convenient way to represent the source data for 3D rendering. Section 5 discusses numerical problems that may arise with this approach, together with three different methods to solve those problems. Finally, examples of 3D rendering in which these solutions are used are shown and discussed in the last sections.

We note that in this article we will not address rendering methods to account for sparkle and other texture effects. This is a separate area, for which improved approaches have been published recently [9][10].

The concept of isochromatic lines

For 3D rendering, it is necessary to find a good representation for the reflectance properties for any combination of the three local angles θ_{ill}, θ_{det} and ϕ_{det}. When BRDF measurements are used, this is done by interpolating the typically hundreds of data points in the three-dimensional space spanned by these three parameters.

However, we will show that with the recently developed methods that introduce flake-based parameters and isochromatic lines (or isolines, in short), it is possible to represent the full BRDF in an effective two-dimensional space, because we are able to convert any out-of-plane geometry into an in-plane geometry, characterized by ϕ_{det} = 0° or 180°, for which the same reflection properties are expected. In a previous publication we showed that this approximation has an average accuracy that ranges from dE_{ab} = 1.2 to 1.6 [11]. For 3D rendering purposes this is considered as highly accurate.

The method to convert a set of values for θ_{ill}, θ_{det} and ϕ_{det}, generally referring to an out-of-plane geometry, into the corresponding in-plane angles θ'_{ill}, θ'_{det} and ϕ'_{det} (with ϕ'_{det} = 0° or 180°) is as follows. The basic idea is that for effect coatings, the relevant physics takes place mainly at the microscopic surface of the flake pigments inside the coating. Therefore the conventional method to express reflection properties as a function of illumination and detection angles (θ_{ill}, θ_{det} and ϕ_{det}) with respect to the normal vector to the macroscopic coating surface is not effective. Instead, it is better to express such properties as a function of angles with respect to the normal vector to the flake pigments. The various parameters are θ_{inc} (angle of incidence with respect to flake normal), θ_{flake} and ϕ_{flake} (polar and azimuthal angle of the flake with respect to coating normal). These parameters are illustrated in Figure 1. We note that the conventional notation of angles also defines the aspecular angle, with

$\theta_{aspec} = \theta_{ill} + \theta_{det}$ if $\phi_{det} = 0°$

$\theta_{aspec} = \theta_{ill} - \theta_{det}$ if $\phi_{det} = 180°$

We also note that this approach may be seen as a variation of microfacet theory, since the reflection from flakes is similar to reflection from the microfacets of a rough surface. Microfacet theory has been used for 3D rendering models such as the Torrance-Sparrow model, the Blinn model and the Ashikhmin-Shirley model [3]. The main difference with microfacet theory is that in the new approach for rendering effect coatings the paint-air interface above the flakes is accounted for.

The derivation of the equations relating both systems of parameters with each other can be found in Refs.[7] [11]. Here, we only present the main equations. We use equations (1) and (2) to calculate the parameters θ_1, θ_2 , which are the angles of incident and exiting light (cf.Fig. 1).

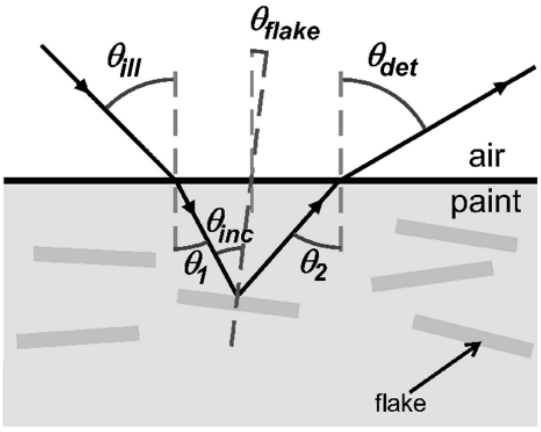

***Figure 1**. Definition of angles for flake-based parameters.*

$$n_{air} \sin\left|\theta_{\det}\right| = n_{coat} \sin\theta_2 \quad (1)$$

$$n_{air} \sin\theta_{ill} = n_{coat} \sin\theta_1 \quad (2)$$

Assuming that only light will reach the detector if it is reflected from a flake inside the paint, we derived expressions to calculate the angle θ_{inc} of the incident light with respect to the flake normal, and the polar and azimuthal angles that determine the orientation of the flake, θ_{flake} and ϕ_{flake}, respectively:

$$\cos\theta_{flake} = \frac{\cos\theta_1 + \cos\theta_2}{\left[2 + 2\sin\theta_1 \sin\theta_2 \cos\phi_{out} + 2\cos\theta_1 \cos\theta_2\right]^{1/2}} \quad (3)$$

$$\cos(2\theta_{inc}) = \sin\theta_1 \sin\theta_2 \cos\phi_{out} + \cos\theta_1 \cos\theta_2 \quad (4)$$

Isolines are defined as the set of measurement geometries for which the parameters θ_{inc} and ϕ_{flake} are constant.

Along an isoline, the parameter ϕ_{flake} is allowed to vary. We will assume that the coating has been applied in such a way that its reflection properties do not change with azimuthal rotation of the sample. Physically, one expects that all measurement geometries on an isoline produce very similar reflection data, because the interesting physical parameters in all those geometries are identical. In a previous publication we showed that this is indeed the case with high accuracy [11].

Generally, the two in-plane geometries on an isoline are found by setting either ϕ_{flake} = 0° or ϕ_{flake} = 180°. With the parameter values for θ_{inc}, θ_{flake} and ϕ_{flake} thus found, we calculate the value of $\cos(\theta'_1)$ by using one of the two roots of eq. (5):

$$\cos\theta'_1 = \frac{\cos\theta_{flake}\cos\theta_{inc} \pm \sin\theta_{flake}\cos\phi_{flake} SQ}{1 - \sin^2\theta_{flake}\sin^2\phi_{flake}} \quad (5)$$

$$SQ = \sqrt{\sin^2\theta_{inc} - \sin^2\theta_{flake}\sin^2\phi_{flake}}$$

Here, θ'_1 is the angle of incidence inside the paint, for the in-plane geometry that falls on the same isoline as the out-of-plane geometry under investigation. The corresponding value for $\sin(\theta'_1)$, including its proper sign, is found from eq. (6).

$$\sin\theta_1' = \frac{\cos\theta_{inc} - \cos\theta_{flake}\cos\theta_1}{\sin\theta_{flake}\cos\phi_{flake}} \quad (6)$$

$$\cos\theta_2' = -\cos\theta_1' + 2T\cos\theta_{flake} \quad (7)$$

$$T = \sin\theta_{flake}\cos\phi_{flake}\sin\theta_1' + \cos\theta_{flake}\cos\theta_1'$$

Using eq.(7), we then calculate $\cos(\theta'_2)$ and hence the value of θ'_2, which is the exit angle of the light inside the paint. By using Snell's law (similar to equations 1 and 2) it is then straightforward to calculate θ'_{ill}, θ'_{det} and ϕ'_{det}, where the latter will be either 0° or 180° because it is an in-plane geometry.

In this way, one in-plane geometry is found. The other in-plane solution is found by either using the other root of eq. (5), or (equivalently) by using the other value of ϕ_{flake} to start with. The two in-plane geometries are related to each other by exchanging detector and illumination, according to the Helmholtz reciprocity principle [11].

Color maps

In order to test the isoline approach for 3D Rendering, we first created a color map that represents the reflection data from a BRDF instrument. From section 2 it is clear that in the isoline approach the reflection data can be expressed as a function of the two parameters θ'_{ill}, and θ'_{det}, which are the illumination and detection angle of the equivalent in-plane geometry. There are two solutions to this procedure, one for ϕ'_{det} = 0° and one for ϕ'_{det} = 180°. Since both solutions coincide for θ'_{det} = 0°, all results can be represented in a single color map as shown in Figure 2.

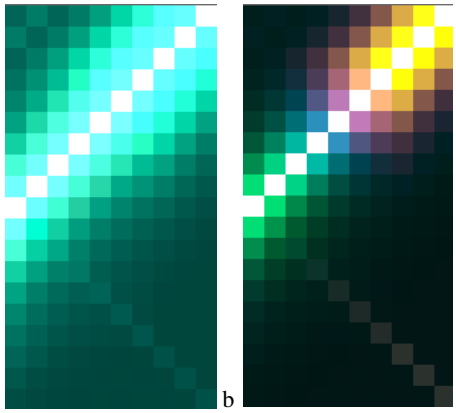

***Figure 2**. Color maps from actual BRDF measurement on (a) typical metallic (sample 7 in Ref.[12]), (b) extreme interference pigment (sample 13). Horizontal axis: parameter cos(θ'ill) Vertical axis: cos(θ'det).*

In Figure 2, the parameters $\cos(\theta'_{ill})$ and $\cos(\theta'_{det})$ are shown on the horizontal and vertical axis, respectively. The top half of the figure shows the case for ϕ'_{det} = 180° (i.e. light source and detector are at opposite sides of the normal vector to the coating), whereas the bottom half corresponds to ϕ'_{det} = 0° (i.e. light source and detector are on the same side). For each point in the graph, we will assume that reflection data is available. This may be direct measurement data from a BRDF instrument, or for example reflection data interpolated from multi-angle spectrophotometer measurements.

In the color map, reflection data is represented by the RGB values of pixels, rather than by the full recorded reflection spectrum for each pixel. This not only makes visualization of the color map much easier, but it is also a necessary step since eventually we need to produce colored RGB-pixels for the rendered image. In the present article, we will use standard sRGB space. Obviously, the isoline method for 3D rendering can be combined with other RGB spaces as well.

The data shown in Figure 2 are actual data from samples 07 and 13 mentioned in Ref.[12], taken with a BRDF instrument. This is the GEFE, the gonio-spectrophotometer developed at the Instituto de Óptica in CSIC (Madrid) [13][14]. It allows the spectral BRDF to be measured at any geometry, including out-of-plane and retro-reflection angles. With this instrument, the polar angles for illumination and detection were sampled in steps of 10°, and the azimuthal angle with steps of 30°. This resulted in reflection data for 448 different geometries for each sample. Details about the measurements and the samples that we investigate here were already published before [12].

In Figure 2, the white diagonal in the top half of each figure is easily identified with angles close to the gloss angle. We will call this white diagonal the gloss line in the color map. From the measurement data shown in Figure 2 the contribution from direct reflection at the air-paint interface (gloss) was already subtracted by calculating the Fresnel equations. If needed, gloss can be explicitly added afterwards in the calculations in the shader, but this was not done for the renderings shown in the present article.

In Figure 2a, we show a color map that is typical for a metallic coating. The sample chosen was a coarse metallic in a green transparent medium (sample 07 in Ref. [12]). The color variation in Figure 2a is mainly due to changes in lightness. Lightness is shown to vary mostly in the direction perpendicular to the gloss line, i.e. along lines for which' $\theta'_{ill} + \theta'_{det}$ is a constant. As we will see below, this is exactly the direction for which the aspecular angle changes most. Therefore Figure 2 confirms that the aspecular angle is an important parameter for describing the angular variation of the color of metallic coatings.

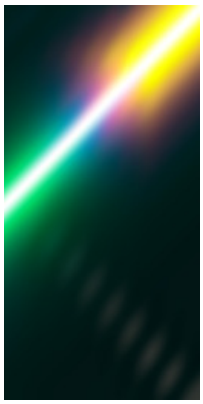

Figure 3. Color map generated for this investigation, based on BRDF measurements on sample 13 of Ref.[12] after bilinear interpolation.

In Figure 2b, a typical color map is shown for an extreme interference pigment. It is a Chromaflair Green Purple pigment (sample 13 in Ref. [12]). In this Figure, we recognize again the lightness variation with aspecular angle that we already discussed for the metallic sample. However, in Figure 2b we see that there is

also a considerable variation in hue and saturation. This variation takes place in a different direction than what can be described with the aspecular angle. Therefore, this Figure already shows that one parameter is not sufficient for describing the full color variation of effect coatings.

For testing and illustrating the new concept for 3D Rendering, we have applied bilinear interpolation on the color map for sample 13 from Ref.[12], that was already shown in figure 2b. This resulted in the color map shown in Figure 3.

Isoline-based 3D Rendering

We have programmed the method of isoline-based 3D Rendering, explained in section 2, in a shader algorithm for 3D rendering. If we apply this shader to the color map shown in Figure 3, the two images shown in Figure 4 are produced. In this case we show a sphere that is illuminated from almost exactly behind the detector (Figure 4a), or from a place somewhere aside (Figure 4b). When the illumination is coming from exactly behind the detector, the 3D Rendering method shows a satisfactory image. In this case the analysis is straightforward, because the symmetry in the set-up shows that for all surface elements of the sphere the local illumination and detection angles are in-plane.

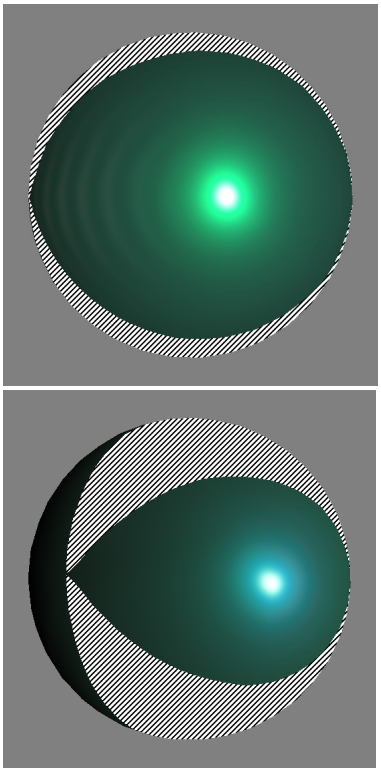

a

b

Figure 4*. Sphere illuminated from (a) almost exactly behind the detector, or (b) more from aside. Both images were generated with the isoline-based 3D rendering method proposed in this article.*

When the light source rotates to a place that is close to but not exactly behind the detector, then the only points on the sphere with local in-plane illumination/detection geometry are the points that lie in the horizontal plane (i.e. the plane containing the detector, the light source and the center of the sphere). Figure 4a shows that the isoline-based 3D rendering method is able to produce a convincing image for many of the other points as well. If only the aspecular angle would have been used, the variation in color hue and saturation would not have been produced. However, near the edges of the sphere the rendering method shows numerical errors. These are indicated by dashed lines in Figure 4a. When the light source moves to a place even further to aside, the area with numerical errors appears becomes larger as shown in Figure 4b. In the next section, we will investigate the origin of and solution to these errors.

Limitations of the isolines concept

The algorithm to calculate θ'_{ill} , θ'_{det} and ϕ'_{det} based on equations (1) to (7) showed error messages in some cases. We found that these errors arise in the final step of the calculation, i.e. after evaluating (7). At that point, in certain cases inside the paint either the angle of incidence θ'_1 or the exit angle θ'_2 exceeds the so-called critical angle.

$$\theta'_{1,2} \geq \theta_{crit} = \arcsin\left(\frac{n_{air}}{n_{coat}}\right) \tag{8}$$

From classical optics it is known that for angles exceeding the critical angle, total reflection occurs at the paint-air interface. This is not accounted for in Snell's equations.

Using Snell's equations (1) and (2), the resulting value for $\sin(\theta'_{ill})$ or $\sin(\theta'_{det})$ would be larger than 1, which makes calculating θ'_{ill} or θ'_{det} mathematically impossible. However, the reason why this computation problem arises is physical in nature. If $\theta'_1 > \theta'_{crit}$, the incident angle inside the paint is so large that according to Snell's law it cannot be the result of refraction from light at the air-paint interface. Therefore this light can only originate from total reflection of light inside the paint, at the paint-air interface. If $\theta'_2 > \theta'_{crit}$, total reflection at the paint-air interface prevents light from leaving the paint. In that case, light needs to be reflected from another flake, or from other reflecting particles in the paint.

Both cases are not described by the simple approximation of single flake scattering that underlies the concepts of flake based parameters and isolines [7]. From Fig. 1 it is clear that the numerical problem arises for geometries that have

$$\theta_{inc} + \theta_{flake} > \arcsin\left(\frac{n_{air}}{n_{coat}}\right) \tag{9}$$

In those cases, we end up with the situation that we need to calculate $\theta'_{ill} = \arcsin(x)$ or $\theta'_{det} = \arcsin(x)$ for a value of $x>1$. We found three solutions for these cases:

A. Clipping by complex analysis

We may use the analytical continuation of the arcsin function in the complex plane as a method to mathematically continue the calculations. For real values of x with $x > 1$,

$$\arcsin(x) = \frac{\pi}{2} - \frac{i}{2}\ln\left|\sqrt{x^2 - 1} + x\right| \tag{10}$$

For 3D rendering applications, the imaginary part of this expression remains much smaller than the real part, and we may consider approximating the full expression by ignoring the imaginary part. In that case, equation (10) shows that we can clip the $\arcsin(x)$ function to 90° in case $x>1$.

From the point of view of optics, this approximation means that we use reflection data that has been measured for the case where θ'_{ill} is close to but smaller than 90°. This data is then

assumed to be also valid for the problematic cases where $\theta'_{ill} > 90°$ (and a similar argument can be made for θ'_{det}) This can be justified because if θ'_{ill} is close to but smaller than 90°, the reflection properties are already dominated by the transparent medium surrounding the flakes, and/or by light having experienced multiple rather than a single reflection from flakes. Since that same situation holds for the case $\theta'_{ill} > 90°$, clipping these expressions at 90° seems to be a valid approximation.

B. Vector analysis in the color map

Cases where $\theta'_{ill} > 90°$ (or $\theta'_{det} > 90°$) are obviously unphysical, because they represent the situation in which the light source (or detector) is positioned below the coating surface. We already saw that complex analysis provides an argument to solve the numerical errors in such cases by clipping the arcsin(x) function. Another solution may be found by calculating cos(θ'_{ill}). For $\theta'_{ill} > 90°$, the cosine can still be calculated. Since the color maps in fact do not show θ'_{det} versus θ'_{ill} , but cos(θ'_{det}) versus cos(θ'_{ill}), this means we are looking for a continuation of the colormap to the right hand side.

As an example, we are interested in describing the colors at points a, b and c in Figure 5. We now see that the clipping method just described means that the colors for these points are taken from points a', b' and c'. However, because of the large role of the aspecular angle in analyzing reflection properties of effect coatings, it may be preferable to take the colors for points a, b, c all from the same point a" instead (or, equivalently, from point e'). This point is found by moving along the aspecular direction (i.e., perpendicular to the gloss line) until we reach the point with $\theta'_{ill} = 90°$. This construction is easily implemented in a shader, as it comes down to a simple vector operation on the color map.

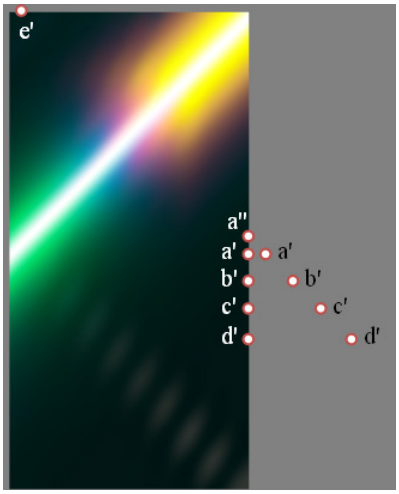

***Figure 5**. Color map illustrating the problem of finding colors for which cos(θ'_{ill})<0.*

C. Removing the critical angle

A third solution to the numerical errors is found by explicitly removing the physical phenomenon that causes them, which is the critical angle. The critical angle appears because the refractive index of the coating (approximately 1.5) differs from the value for air. As an alternative method to remove numerical errors, we can numerically change the refractive index to 1.0.

Discussion

All three approaches are numerically feasible, and can be programmed in a shader for 3D rendering. They all represent approximations that are added to the physical assumptions on which the concepts of flake-based parameters and isolines are based. The numerical errors that these approaches aim to solve do not occur for the vast majority of out-of-plane geometries, and if they do occur this usually happens for geometries for which rather dark reflections are expected. The numerical errors do not occur in regions closer to the highlights in a 3D rendering scene, except in the top-right area of the color map. This area refers to situations in which θ'_{det} and θ'_{ill} are both slightly smaller than 90°. This occurs for surface elements positioned almost exactly between the light source and the detector, with light incident on a locally very oblique, grazing angle. This is a situation where the color of an automotive coating is very hard to judge, and has little impact on the perceived color accuracy of the rendering. Therefore we think it is fair to make these assumptions in 3D rendering applications.

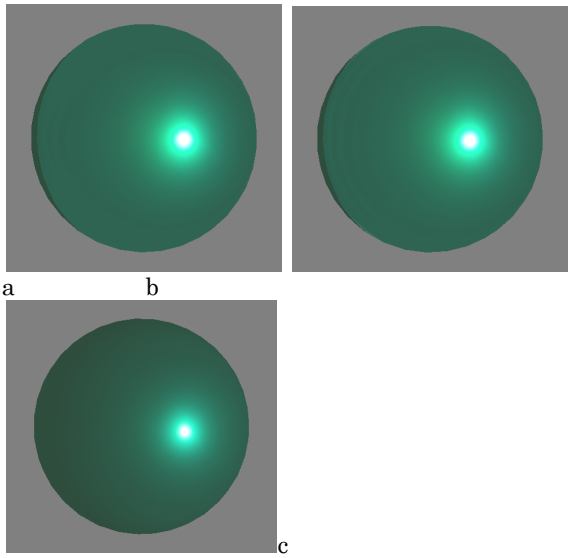

***Figure 6**. Examples of sphere rendered with methods proposed in this article, using (a) method A: clipping, (b) method C :removing the critical angle, and (c) method A and also accounting for projected solid angles.*

Examples of the resulting rendering are shown in Figure 6a, 6b and 6c. All three figures show practically the same rendering scene as in Figure 4b. The numerical errors that plagued Figure 4b are shown to be solved in an aesthetically convincing way. In Figure 6a this is accomplished by method A (clipping), whereas in Figure 6b this is realized by method C (removing the critical angle). Although a close investigation does reveal differences between Figure 6a and 6b, it is clear that both approaches lead to very similar renderings. In Figure 6c we have also accounted for the projection factor of solid angles, which decreases the contrast on the borderline between highlighted and shadowed parts of the sphere.

Conclusions

In summary, we conclude that we have found an approach to 3D rendering in which the many out-of-plane geometries that are met during rendering can be effectively mapped onto equivalent in-plane geometries. Instead of needing three dimensions (θ_{ill}, θ_{det} and ϕ_{det}) to characterize the local illumination and detection geometry at a surface element, we found that it is possible to use only two dimensions (θ'_{ill} and θ'_{det}). This makes the use of Look Up Tables in 3D rendering applications much faster, because we now need interpolation in two rather than three dimensions.

With the isoline-based rendering approach, real time rendering becomes possible without needing the rather crude physical models that are currently used for rendering effect coatings. In Figure 7 we show two rendering examples, illustrating the new method for a typical metallic coating (sample 7 of Ref.[12]) and a typical extreme interference coating (sample 13). The lightness gradient for the metallic sample produced by the isoline-based rendering method is significantly different from gradients found with conventional rendering models. For the extreme interference coating, the new method is able to capture the hue gradient that is characteristic for this type of coatings.

The method was illustrated in combination with sRGB color space, but it is equally applicable in combination with any other color space. We note here that the rendering method proposed in this article can also be used to characterize the angular dependence of the reflective properties of effect coatings by much fewer measurement geometries than by a full BRDF. The method is applicable to any gonio-apparent coating that is based on flake pigments. For example, standard practice in automotive and paint industry is to characterize metallic paints by reflection measurements under three different geometries [15][16]. Three more geometries are added to also characterize pearlescent coatings [7]. Therefore common multi-angle spectrophotometers address only a few geometries, and all these geometries are in-plane. With isolines we can use such in-plane reflectance data to find approximate but highly accurate reflectance values for any (in-plane and out-of-plane) geometry [17]. We plan to investigate this approach further in the future.

Acknowledgments

Authors are grateful to EMRP for funding the project "Multidimensional reflectometry for industry". The EMRP is jointly funded by the EMRP participating countries within EURAMET and the European Union. Authors are also grateful to Comunidad de Madrid for funding the project SINFOTON-CM: S2013/MIT-2790.

References

[1] J. Günther, T. Chen, M. Goesele, I. Wald and H.P. Seidel. Efficient acquisition and realistic rendering of car paint. In: G. Greiner, J. Hornegger, H. Niemann and M. Stamminger, eds., Proc. Vision, Modeling and Visualization (VMV'05):487-494, 2005.

[2] J.A. Ferwerda, S.H. Westin, R.C. Smith and R. Pawlicki. Effects of rendering on shape perception in automobile design. Proc. ACM Symposium on applied perception in Graphics and Visualization:107-114, 2004.

[3] M. Pharr and G. Humphreys. Physically based rendering (Elsevier, 2010).

[4] C. Shimizu, G.W. Meyer and J.P. Wingard. Interactive goniochromatic color design. In: Proc. IS&T/SID's Eleventh Color Imaging Conference:16-22, 2003.

[5] G.W. Meyer and C. Shimizu. Computational automotive color appearance. In: L. Neumann, M. Sbert, B. Gooch and W. Purgathofer, eds., Computational Aesthetics 2005: Eurographics workshop on Computational Aesthetics in Graphics, Visualization and Imaging. (Eurographics association):217-222, 2005.

[6] P. Dumont-Bècle, E. Ferley, A. Kemeny, S. Michelin and D. Arquès. Multi-texturing approach for paint appearance on virtual vehicles. Proc. Driving Simulation Conference:123-133, 2001.

[7] E.J.J. Kirchner and W.R. Cramer. Making sense of measurement geometries for multi-angle spectrophotometers. Color Res. Appl. 37:186-198, 2012.

[8] W.R. Cramer. Examples of interference and the color pigment mixtures green with red and red with green. Color Res. Appl. 27:276-281, 2002.

[9] I.B.N. van der Lans, E.J.J. Kirchner, A. Half. Accurate appearance-based visualization of car paints. Proc. Col. Graph. Img. Vis.(CGIV):17-23, 2012.

[10] A. Ferrero, J. Campos, A.M. Rabal, A. Pons. A single analytical model for sparkle and graininess patterns in texture of effect coatings. Opt. Exp. 21:26812-26819, 2013.

[11] E. Kirchner and A. Ferrero, Isochromatic lines as extension of Helmholtz reciprocity principle for effect paints. J. Opt. Soc. Am. A 31:1861-1867, 2014.

[12] A. Ferrero, B. Bernad, J. Campos, F.M. Martínez-Verdú, E. Perales, I. van der Lans and E. Kirchner. Towards a better understanding of the color shift of effect coatings by densely sampled spectral BRDF measurement. Proc. SPIE-IS&T Electronic Imaging conference, SPIE Vol. 9018, 2014.

[13] A. Ferrero, E. Perales, A.M. Rabal, J. Campos, F.M. Martínez-Verdú, E. Chorro and A. Pons. Color representation and interpretation of special effect coatings. J. Opt. Soc. Am. A 31:436-447, 2014.

[14] A.M. Rabal, A. Ferrero, J. Campos, J.L. Fontecha and A. Pons. Automatic gonio-spectrophotometer for the absolute measurement of the spectral BRDF at in- and out-of-plane and retroreflection geometries. Metrologia 49: 213-223, 2012.

[15] D.H. Alman. Directional color measurement of metallic flake finishes. Proc. Inter-Society Color Council Conference on Appearance, Williamsburg:53-56, 1987.

[16] H.J.A. Saris, R.J.B. Gottenbos and H. van Houwelingen. Correlation between visual and instrumental colour differences of metallic paint films. Color Res. Appl. 15:200-205, 1990.

[17] A. Ferrero, J. Campos, E. Perales, F.M. Martínez-Verdú, I. van der Lans and E. Kirchner. Global color estimation of special-effect coatings from measurements by commercially available portable multiangle spectrophotometers. J. Opt. Soc. Am. A 32:1-11, 2015.

Author Biography

Eric Kirchner received his PhD in theoretical chemistry from the Free University of Amsterdam (1993). Since 2000 he has worked on colorimetry in AkzoNobel. His work has focused on modeling, measurement, accurate displaying and perception of color and texture.

a

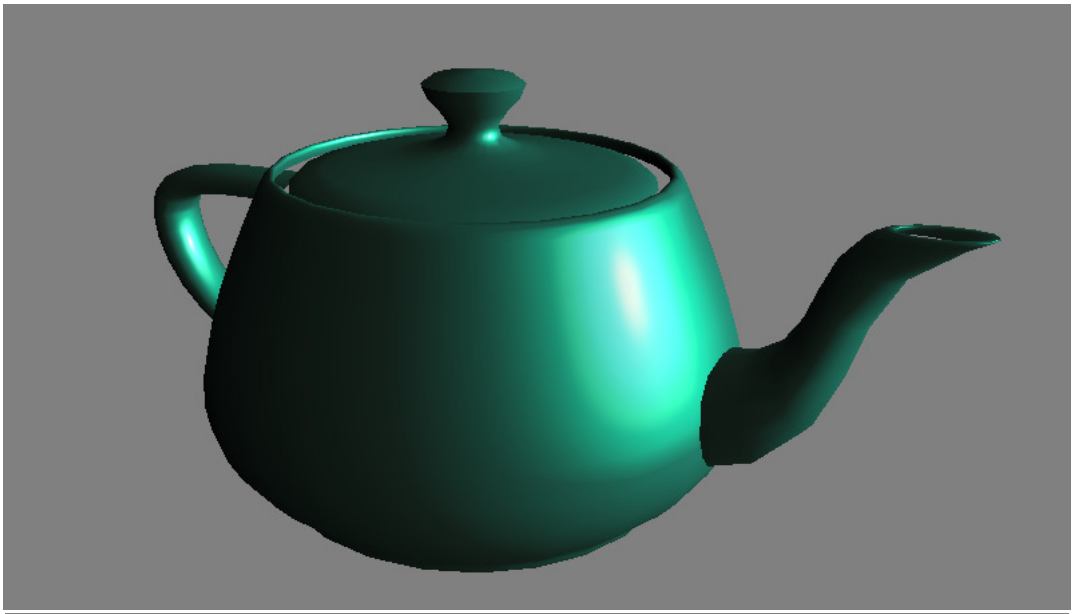

b

Figure 7*. In these 3D rendering examples of the Utah teapot we used the isoline-based rendering method developed in this article, using the proposed clipping method. Color information is based on the BRDF measurements on metallic sample 7 from Ref.[12], and extreme interference sample 13.*